American Mineralogist, Volume 77, pages 512–521, 1992

Single-crystal X-ray structure study of synthetic pyrope almandine garnets at 100 and 293 K

THOMAS ARMBRUSTER
Laboratorium für chemische und mineralogische Kristallographie, Universität Bern, CH-3012 Bern, Freiestrasse 3, Switzerland
CHARLES A. GEIGER*
Bayerisches Geoinstitut, Universität Bayreuth, Postfach 10 12 51, D-8580 Bayreuth, Germany
GEORGE A. LAGER
Department of Geology, 325 Natural Science Building, University of Louisville, Louisville, Kentucky 40292, U.S.A.

ABSTRACT

The crystal structures of synthetic pyrope ($Mg_3Al_2Si_3O_{12}$), almandine ($Fe_3Al_2Si_3O_{12}$), and the solid-solution garnet compositions Py_{80}-Alm_{20}, Py_{60}-Alm_{40}, and Py_{20}-Alm_{80} have been refined in space group $Ia\bar{3}d$ from high-precision X-ray diffraction data with $\sin\theta/\lambda > 0.4$ Å^{-1} measured at 100 and 293 K. There is no indication of lower symmetry for pyrope, almandine, or solid-solution members. Experimentally determined atomic coordinates and displacement parameters for the solid-solution compositions are in good agreement with those linearly interpolated from the end-members. Thus there are no apparent structural features that could account for substantial nonideal enthalpies of mixing in the system pyrope-almandine. The tetrahedral rotation angle is inversely correlated with the X-O distance. Fe^{2+} substitution on the eight-coordinated X site of pyrope, or increasing temperature, decreases the rigid tetrahedral rotation in garnet. The large and anisotropic displacement parameters for the X-site cations in garnet are mainly a result of anisotropic thermal vibrations along the longer X-O bonds, which produce nonrigid polyhedral behavior for the dodecahedral site. The tetrahedra and octahedra behave as rigid bodies. These strong vibrations of the former give rise to the relatively large heat capacities and third-law entropies in garnet. Previous proposals concerning subsite dodecahedral ordering in pyrope must be revised.

INTRODUCTION

Pyrope-almandine solid solutions represent the petrologically and geophysically most important garnets in the Earth's crust and uppermost mantle. Therefore a detailed understanding of their thermodynamic and structural properties is essential for quantitative geophysical and geochemical calculations.

The general structural formula of garnet can be expressed as $\{X_3\}[Y_2](Z_3)O_{12}$, where { } refers to an eight-coordinated dodecahedral site (Wyckoff position 24c), [ ] to an octahedral site (16a), and ( ) to a tetrahedral position (24d). Naturally occurring garnets are commonly complex solid solutions of several components and cation ordering may lead in a few cases to a symmetry lower than the parent space group $Ia\bar{3}d$ (Menzer, 1928; Geller, 1967). In particular, members of the andradite-grossular series (X = Ca and Y = Fe^{3+}, Al) may display anisotropic optical properties that have been related to cation ordering on the octahedral and dodecahedral sites (Takéuchi et al., 1982; Allen and Buseck, 1988; Kingma and Downs, 1989). To date, only one example for site ordering of different divalent cations in natural aluminosilicate garnets where Y = Al (X = Mg for pyrope, X = Fe^{2+} for almandine, X = Ca for grossular, X = Mn^{2+} for spessartine) has been demonstrated. Griffin et al. (1990) refined the structure of a tetragonal, optically birefringent garnet of the composition $\{Fe_{1.881}Ca_{0.753}Mg_{0.239}Mn_{0.103}\}_{\Sigma=2.976}[Al_{1.963}Fe_{0.031}Ti_{0.007}]_{\Sigma=2.001}Si_{3.011}O_{12}$ and determined slight ordering of Ca and (Fe,Mg,Mn) on the X site. Previously Dempsey (1980) proposed that Mg-Ca ordering could be present in a synthetic garnet of composition $Py_{90}Gr_{10}$.

Zemann and Zemann (1961) and Gibbs and Smith (1965) refined the structure of pyrope at room temperature, and the former authors suggested that the Mg cation may be slightly disordered in the direction of the electron density anisotropy. A strong anisotropy was also confirmed by Gibbs and Smith (1965), and they suggested that the small Mg cation occupied the large dodecahedral site with a strong anisotropic vibration. Temperature-dependent (298, 623, 823, and 1023 K) X-ray structure investigations have also been carried out on synthetic pyrope (Meagher, 1975). However, the results of Meagher (1975) do not allow a decision to be made regarding whether multiple sites exist at low temperatures.

The structures of two natural almandine-rich solid-solution compositions were refined by Prandl (1971) and Novak and Gibbs (1971). Geiger et al. (1992) carried out

* Present address: Mineralogisch-Petrographisches Institut, Universität Kiel, Olshausenstraße 40, 2300 Kiel, Germany.

0003–004X/92/0506–0512$02.00

refinements on end-member almandine at 100, 293, 420, and 500 K, and these temperature-dependent refinements, with anisotropic displacement parameters, showed no off-center positions for eight-coordinated Fe^{2+} but confirmed strongly anisotropic thermal motion.

Considerable confusion presently exists as to whether the Mg cation in pyrope displays dynamic disorder or is statistically distributed on several subsites around the 24c position. Kleber et al. (1969) suggested on the basis of an X-ray structural investigation of natural pyrope $\{Mg_{2.0}Fe_{0.7}Ca_{0.3}\}[Al_{1.7}Cr_{0.1}Fe_{0.1}Ti_{0.1}](Si_{2.9}Al_{0.1})O_{12}$ that the X cation position, with local 222 symmetry, splits into four statistically occupied general positions located ± 0.07 Å from the symmetry-fixed special site (24c). Two arguments were proposed to support the split cation positions: (1) difference-Fourier syntheses obtained from refinements with isotropic displacement parameters yielded residual density around the special position and (2) small isotropic atomic displacements seemed to exclude anharmonic vibrations. Cressey (1981) extended this concept in his interpretation of the configurational entropies of mixing for almandine-grossular solid solutions. The presence of different subsites within the dodecahedral site would have an important influence on the configurational entropies of mixing and hence the stability of garnet. The behavior of the Mg cation in pyrope and its relation to the large heat capacity of that mineral were also addressed by Kieffer (1980) and Hofmeister and Chopelas (1991). Haselton and Westrum (1980) concluded from their low-temperature adiabatic measurements of heat capacity of pyrope that there was no evidence for subsite disorder.

A model for off-center displacement of cations was introduced by Megaw (1968) for cations in octahedral coordination, but it may also be extended to higher coordinations. Potential energy and force-field considerations show that in a large coordination polyhedron (e.g., the dodecahedral site in garnet) small cations like Mg and Fe^{2+} could be located on off-center positions. Thus, a static-position or space-averaged displacement offers an alternative model to a dynamic, time-averaged disorder or a rattling effect. Provided that the static-position displacement is disordered, the two effects can only be distinguished on the basis of temperature-dependent structural investigations, as has been done in the case of albite (Winter et al., 1977). Position disorder is expected to be temperature independent, whereas a time-averaged vibration should be dependent on temperature.

In this X-ray study we have chosen 100 K and room temperature as measuring conditions because high precision and excellent data quality can be achieved. In addition to this single-crystal diffraction investigation, temperature-dependent spectroscopic (IR and NMR) measurements have been made on pyrope synthesized at very high temperatures in an accompanying study (Geiger et al., in preparation). The underlying crystal-chemical rationale for undertaking the low-temperature measurements is as follows. First, a structural explanation is sought for the relatively high third-law entropies that have been measured and calculated for end-member pyrope and almandine garnets. Moreover, the measurements of Haselton and Westrum (1980) indicate that excess third-law entropies of mixing may originate at relatively low temperatures for solid-solution compositions. Second, in examining the garnet solid solutions in a systematic way across the join, we seek a structural explanation for the asymmetric excess enthalpies of mixing that may exist for almandine-pyrope-garnet solid solutions. It has been proposed that $(Fe^{2+},Mg)_3Al_2Si_3O_{12}$ solid solutions exhibit positive excess enthalpies of mixing (Ganguly and Saxena, 1984; Geiger et al., 1987). However, the calorimetric measurements can also be fitted within their error bars to an ideal or nearly ideal mixing model (Geiger, 1986; Berman, 1990). Structural strains have been invoked to explain the excess enthalpies of mixing in silicate solid solutions, and therefore a careful X-ray study of well-characterized synthetic almandine pyrope garnets could provide such structural information.

TABLE 1. Synthesis conditions of garnet single crystals

Composition	Starting material	Synthesis conditions	P (kbar) T (°C)	Duration (h)
Pyrope	oxide mix	excess SiO_2	21 1000	19
Py_{80}-Alm_{20}	gel	Fe-FeO buffer	22 950	5
Py_{60}-Alm_{40}	gel	Fe-FeO buffer	12 800	20
Py_{20}-Alm_{80}	gel	in Fe capsule	18 900	17
Almandine	oxide mix	in Fe capsule	15 850	24

EXPERIMENTAL PROCEDURE

The garnet crystals investigated were grown hydrothermally at high temperatures and pressures in a piston-cylinder device. The synthesis conditions are listed in Table 1. All X-ray single-crystal data were measured using an Enraf-Nonius CAD4 diffractometer (graphite monochromated Mo$K\alpha$ X-radiation) at 100 K and at room temperature (RT = 293 K). Low temperatures (100 K) were achieved with a conventional liquid N_2 cooling device with an accuracy of ± 2 K. The mean diameter of the crystals was between 0.07 and 0.85 mm depending on the synthesis conditions and composition (Table 2). All Fe-containing garnets were yellow–light brown in color, appeared isotropic when examined with a polarizing microscope, and did not show any indication of compositional zoning. The ω-θ profile scans over strong reflections did not show any differences in peak shape between the end-members and solid-solution members, thus supporting the homogeneous chemical character of the crystals. A low degree of crystal mosaicity (leading to extinction problems) was indicated by the sharpness of the reflections. The unit-cell parameters for all crystals were determined from least-squares refinements of automati-

TABLE 2. Experimental conditions for X-ray single-crystal data measurement of almandine pyrope garnets

	Pyrope	Py_{80}-Alm_{20}	Py_{60}-Alm_{40}	Py_{20}-Alm_{80}	Almandine
Crystal size (mm)	0.45/0.85	0.10	0.22	0.07	0.37
Cell dimension 100 K	11.441(1)	11.458(2)	11.471(2)	11.502(2)	11.512(1)
293 K	11.452(1)	11.473(2)	11.485(2)	11.516(2)	11.525(1)
Scan mode	ω-θ	ω-θ	ω-θ	ω-θ	ω-θ
Scan angle + 0.35 sin(θ)	2.0	2.0	2.0	2.0	2.5
Max scan time (s)	120	300	200	500	360
Upper θ limit 100/293 K	60/50	55/55	40/40	55/55	55/50
Measured intensities 100 K	5643	794	665	342	2828
Measured intensities 293 K	4214	1059	902	320	2207
Agreement factor					
on intensities 100 K	1.2	3.0	2.8	1.5	2.6
293 K	1.5	2.6	1.3	1.5	1.5
Symmetry-independent accepted reflections					
$F_{obs} > 6\sigma(F_{obs})$ 100 K	729	146	y197	128	490
293 K	544	134	178	112	387
R (%) 100 K	1.1	1.1	2.4	1.2	1.9
R_w (%) 100 K	1.5	1.4	2.3	1.5	1.9
R (%) 293 K	1.2	1.3	1.1	1.3	1.3
R_w (%) 293 K	1.7	1.5	1.4	1.5	1.7

Note: $R = \Sigma\|F_{obs}| - F_{calc}\|/\Sigma|F_{obs}|$, $R_w = (\Sigma w(|F_{obs}| - |F_{calc}|)^2/\Sigma w|F_{obs}|^2)^{1/2}$.

cally centered reflections (20,0,0; 16,16,0; and their symmetric equivalents).

The data measurement and analysis were complicated by the effects of multiple diffraction (e.g., Euler and Bruce, 1965; Prandl, 1971), which gave rise to apparent space-group violations and increased intensities of some reflections. To circumvent this problem, at least two sets of symmetry-equivalent reflections were measured in two different octants of reciprocal space (six sets for large crystals). To save time during data measurement, one complete set of unique reflections (assuming I centering) was measured at RT for Py_{80}-Alm_{20} and Py_{60}-Alm_{40}. In the second set, only those reflections were measured where significant intensity [$I > 3\sigma(I)$] was observed in the first set. Only the intensities of reflections with significant intensity at RT were measured at 100 K. These procedures seemed justified because reflections with $F_{obs} < 6\sigma(F_{obs})$ were rejected for the refinement. Data sets for various octants were empirically corrected for absorption (ψ scans) and subsequently compared. For those reflections in which intensity differences $|I1 - I2| > 7\sigma(I)$ were observed, a test for multiple reflection (ψ scan) was carried out. In all cases, these intensity differences were related to multiple diffraction and the reflection was eliminated from the data set. The larger σ, either from averaging or counting statistics, was used as the standard deviation. Additional experimental details are given in Table 2 and for end-member almandine in Geiger et al. (1992).

Data reduction, including background and Lorentz polarization corrections, were carried out with the SDP (Enraf-Nonius, 1983) program library. To exclude effects related to bonding electrons (Hirshfeld, 1976), reflections with $\sin\theta/\lambda < 0.4$ Å^{-1} were not included in the refinement model. In addition, reflections with $F_{obs} < 6\sigma(F_{obs})$ were rejected. Structure-factor amplitudes were weighted at $1/\sigma^2$. Neutral atom scattering factors with corrections for anomalous dispersion were used (Ibers and Hamilton, 1974). In the final cycles a total of 18 variables, comprising a scale factor, extinction factor, three positional displacement parameters, and 13 anisotropic displacement parameters, were refined (Zucker et al., 1983). Table 3[1] contains a list of observed and calculated structure factors. The chemical compositions of the garnets were fixed at the intended starting compositions of the syntheses. In addition, in previous test refinements (not summarized in Tables 4a, 4b) the (Mg,Fe) population on the X site and the (Fe,Al) population on the Y site were also refined.

RESULTS AND DISCUSSION

Final positional and anisotropic displacement parameters are given in Tables 4a and 4b. Interatomic distances, angles, and distortion parameters are given in Table 5. The test refinements with $\sin\theta/\lambda > 0.4$ Å^{-1} indicated that the refined (Mg,Fe) populations are within 2σ (1σ = 1–2%) of the starting composition of the syntheses. Because of the high correlation among the (Mg,Fe^{2+}) population, scale factor, extinction factor, and displacement parameters, the (Mg,Fe^{2+}) occupancy was fixed at a prescribed value (i.e., the synthesis composition).

The most precise structural data were obtained for pyrope and almandine because these end-member compositions yielded the largest single crystals and thus a high upper θ limit could be chosen. The (Fe,Al) population refinements for almandine yielded 99.9(6)% Al in octahedral coordination. For the solid-solution members, a maximum octahedral Fe content of 2(1)% was initially

[1] To receive a copy of Table 3, order Document AM-92-494 from the Business Office, Mineralogical Society of America, 1130 Seventeenth Street NW, Suite 330, Washington, DC 20036, U.S.A. Please remit $5.00 in advance for the microfiche.

TABLE 4A. Observed and interpolated positional and displacement parameters of almandine pyrope garnets at 100 K

Coord. U_{ij}	Pyrope	Py_{80}-Alm_{20}	Py_{60}-Alm_{40}	Py_{20}-Alm_{80}	Almandine
			O		
x	0.03292(1)	0.03295(7)	0.03327(7)	0.0335(1)	0.03395(3)
		0.03314*	0.03336*	0.03380*	
y	0.05067(1)	0.05062(8)	0.05031(7)	0.0499(1)	0.04943(3)
		0.05041*	0.05014*	0.04961*	
z	0.65333(1)	0.65326(8)	0.65291(7)	0.6530(1)	0.65268(4)
		0.65321*	0.65309*	0.65285*	
B_{eq}	0.246(1)	0.249(9)	0.21(1)	0.25(1)	0.221(4)
U_{11}	0.00313(4)	0.0037(3)	0.0024(4)	0.0034(4)	0.0028(1)
		0.0031*	0.0030*	0.0029*	
U_{22}	0.00370(4)	0.0034(3)	0.0031(4)	0.0035(4)	0.0032(1)
		0.0036*	0.0035*	0.0034*	
U_{33}	0.00252(4)	0.0024(3)	0.0023(3)	0.0025(4)	0.0024(1)
		0.0025*	0.0025*	0.0025*	
U_{12}	0.00043(2)	0.0001(2)	0.0005(3)	0.0002(4)	0.0006(1)
		0.0005*	0.0005*	0.0006*	
U_{13}	−0.00062(2)	−0.0005(2)	−0.0009(2)	−0.0005(4)	−0.0007(1)
		−0.0006*	−0.0007*	−0.0007*	
U_{23}	0.00000(2)	0.0001(2)	−0.0002(2)	−0.0005(4)	−0.0000(1)
		0.0000*	0.0000*	−0.0001*	
		Mg,Fe (0,¼,⅛) $U_{11} = U_{22}$; $U_{13} = U_{23} = 0$			
B_{eq}	0.338(4)	0.28(1)	0.268(6)	0.21(1)	0.215(1)
U_{11}	0.00506(4)	0.0043(4)	0.0043(2)	0.0034(3)	0.00335(5)
		0.0047*	0.0044*	0.0038*	
U_{33}	0.00274(5)	0.0021(4)	0.0016(2)	0.0011(3)	0.00129(6)
		0.0025*	0.0022*	0.0017*	
U_{12}	0.00119(3)	0.0000(3)	0.0004(2)	0.0001(4)	0.00026(4)
		0.0010*	0.0008*	0.0003*	
		Al (0,0,0) $U_{11} = U_{22} = U_{33}$; $U_{12} = U_{13} = U_{23}$			
B_{eq}	0.166(2)	0.128(3)	0.103(6)	0.15(1)	0.119(2)
U_{11}	0.00210(3)	0.0016(1)	0.0014(2)	0.0020(1)	0.00151(7)
		0.0020*	0.0019*	0.0017*	
U_{12}	0.00000(2)	−0.0002(2)	−0.0001(2)	−0.0012(5)	0.00006(6)
		0.0001*	0.0002*	0.0002*	
		Si (⅜,0,¼) $U_{22} = U_{33}$; $U_{12} = U_{13} = U_{23} = 0$			
B_{eq}	0.145(4)	0.14(1)	0.10(1)	0.19(2)	0.107(4)
U_{11}	0.00166(4)	0.0015(3)	0.0009(3)	0.0025(7)	0.0012(1)
		0.0016*	0.0015*	0.0013*	
U_{22}	0.00192(3)	0.0020(2)	0.0015(2)	0.0023(5)	0.00141(8)
		0.0018*	0.0017*	0.0015*	

Note: $B_{eq} = \frac{8}{3}\pi^2\Sigma_i[\Sigma_j(U_{ij}a_i^*a_i^*a_ia_j)]$; displacement parameters are of the form $\exp[-2\pi^2(U_{11}h^2a^{*2} + U_{22}k^2b^{*2} + U_{33}l^2c^{*2} + 2U_{12}hka^*b^* + 2U_{13}hla^*c^* + 2U_{23}klb^*c^*)]$.

* Interpolated parameters.

refined. Because these Fe concentration levels were not considered significant, complete Al occupancy was assumed in all subsequent cycles. The atomic coordinates, bond lengths, and bond angles at 293 K determined for pyrope in this study are in good agreement with those of the refinements of Novak and Gibbs (1971) and Meagher (1975). However, highly significant differences exist for displacement parameters. The present study also yielded much lower standard deviations for all refined parameters.

Deviation from $Ia\bar{3}d$ symmetry?

Extreme caution must be exercised in interpreting the diffraction data in garnet because of the strong influence of multiple diffraction on weak or $Ia\bar{3}d$-forbidden reflections. In particular, reflections caused by multiple diffraction may incorrectly suggest a lower space group than $Ia\bar{3}d$. If significant intensity differences were observed between symmetrically equivalent reflections or if diffraction intensity was detected for $Ia\bar{3}d$-forbidden reflections, then the corresponding reflections were either tested experimentally using ψ scans or ψ-scan profiles were calculated with the program PSIINT (Rossmanith et al., 1990). If the reflection intensities were not influenced by multiple reflection and if anisotropic absorption could be ruled out, the intensities should be independent of the ψ angle. The strong ψ dependence of the intensities for the high-angle reflection 10,10,2 that is forbidden by the space group $Ia\bar{3}d$ (Fig. 1) is characteristic of severe multiple reflection. The good agreement between calculated and measured ψ scans (Fig. 1) underlines the equivalence of both tests. The application of such tests to all suspect reflections confirmed that all pyrope almandine garnets exhibited $Ia\bar{3}d$ space group symmetry.

Yakel and Fankuchen (1962) demonstrated that for equiinclination Weissenberg geometry multiple reflection

TABLE 4B. Observed and interpolated positional and displacement parameters of almandine pyrope garnets at 293 K

Coord. U_{ij}	Pyrope	Py_{80}-Alm_{20}	Py_{60}-Alm_{40}	Py_{20}-Alm_{80}	Almandine
			O		
x	0.03290(2)	0.03313(9)	0.03337(5)	0.0339(1)	0.03401(3)
		0.03312*	0.03334*	0.03378*	
y	0.05034(2)	0.05019(9)	0.04986(5)	0.0491(2)	0.04901(4)
		0.05007*	0.04981*	0.04928*	
z	0.65330(2)	0.65329(9)	0.65306(5)	0.6529(2)	0.65278(4)
		0.65320*	0.65309*	0.65288*	
B_{eq}	0.376(2)	0.39(1)	0.405(8)	0.45(2)	0.344(2)
U_{11}	0.0048(1)	0.0053(3)	0.0050(2)	0.0048(5)	0.0042(1)
		0.0047*	0.0046*	0.0043*	
U_{22}	0.0059(1)	0.0056(3)	0.0065(2)	0.0072(6)	0.0057(1)
		0.0059*	0.0058*	0.0057*	
U_{33}	0.0036(1)	0.0038(3)	0.0040(2)	0.0049(5)	0.0033(1)
		0.0035*	0.0035*	0.0034*	
U_{12}	0.0009(1)	0.0010(3)	0.0009(1)	0.0006(5)	0.0013(1)
		0.0011*	0.0011*	0.0012*	
U_{13}	−0.0011(1)	−0.0011(2)	−0.0009(1)	−0.0014(4)	−0.0013(1)
		−0.0011*	−0.0011*	−0.0012*	
U_{23}	−0.0002(1)	0.0002(3)	−0.0001(1)	−0.0001(5)	−0.0004(1)
		−0.0002*	−0.0003*	−0.0004*	
			Mg,Fe (0,¼,⅛) $U_{11} = U_{22}$; $U_{13} = U_{23} = 0$		
B_{eq}	0.665(2)	0.63(2)	0.616(5)	0.53(1)	0.462(2)
U_{11}	0.0104(2)	0.0099(3)	0.0095(2)	0.0081(5)	0.00747(6)
		0.0098*	0.0092*	0.0081*	
U_{33}	0.0045(1)	0.0041(4)	0.0045(2)	0.0037(5)	0.00261(6)
		0.0041*	0.0037*	0.0030*	
U_{12}	0.0031(2)	0.0017(4)	0.0015(1)	0.0005(5)	0.00088(6)
		0.0027*	0.0020*	0.0014*	
			Al (0,0,0) $U_{11} = U_{22} = U_{33}$; $U_{12} = U_{13} = U_{23}$		
B_{eq}	0.248(2)	0.233(4)	0.255(4)	0.266(6)	0.211(2)
U_{11}	0.0031(1)	0.0029(1)	0.0032(1)	0.0034(2)	0.00267(8)
		0.0030*	0.0029*	0.0028*	
U_{12}	0.0000(1)	0.0001(3)	0.0000(1)	−0.0008(6)	0.0001(1)
		0.0000*	0.0000*	0.0001*	
			Si (⅜,0,¼) $U_{22} = U_{33}$; $U_{12} = U_{13} = U_{23} = 0$		
B_{eq}	0.220(4)	0.22(2)	0.241(8)	0.30(4)	0.172(4)
U_{11}	0.00245(5)	0.0026(4)	0.0027(2)	0.0031(7)	0.0017(1)
		0.0023*	0.0022*	0.0019*	
U_{22}	0.00296(5)	0.0029(2)	0.0032(1)	0.0041(6)	0.00240(9)
		0.0028*	0.0027*	0.0025*	

Note: $B_{eq} = 8/3\pi^2\Sigma_i[\Sigma_j(U_{ij}a_i^*a_i^*a_ia_j)]$; displacement parameters are of the form $\exp[-2\pi^2(U_{11}h^2a^{*2} + U_{22}k^2b^{*2} + U_{33}l^2c^{*2} + 2U_{12}hka^*b^* + 2U_{13}hla^*c^* + 2U_{23}klb^*c^*)]$.

* Interpolated parameters.

is a systematic effect, especially if a reciprocal axis is mounted parallel to the rotation axis. Euler and Bruce (1965) addressed the multiple-diffraction problem for garnets and gave additional details on how reflections should be examined using a Weissenberg camera to avoid misinterpretation of observed intensities. Dempsey's (1980) proposal for possible cation ordering in space group $I2_13$ for a synthetic $pyrope_{90}$-$grossular_{10}$ crystal studied with an oscillation camera should therefore be regarded with skepticism, as should Cressey's (1981) preliminary call for a space group of lower symmetry in natural almandine pyrope garnets. Recent work does however show that certain end-member garnets may deviate slightly from cubic symmetry. Dong and Lu (1991) have presented EXAFS results that indicate that some rare earth garnets are best described by $R\bar{3}$ space group symmetry as a result of small exchanges between dodecahedral and octahedral cations and small displacements of atomic positions. For the aluminosilicate garnets, it is known that small amounts of Fe^{2+} can occur in octahedral coordination in calcium titanium garnets (Kühberger et al., 1989) and in high-pressure silica-rich garnets of pyroxene stoichiometry (Geiger et al., 1991), but it has not been demonstrated that Al can occur in dodecahedral coordination. Moreover, no octahedral off-symmetry positions have been detected using single-crystal X-ray techniques.

Structural distortions

To test whether the solid-solution members show any structural deviation (i.e., distortion) from an ideal pyrope-almandine mixture, positional and displacement parameters were linearly interpolated for the solid-solution members—Py_{80}-Alm_{20}, Py_{60}-Alm_{40}, and Py_{20}-Alm_{80}—from the end-members (Tables 4a, 4b). The agreement between the interpolated and the experimentally observed O coordinates for all three intermediate compo-

TABLE 5. Interatomic distances (Å), O-M-O angles, and polyhedral distortions at 100 and 293 K

	Pyrope 100 K 293 K	Py_{80}-Alm_{20} 100 K 293 K	Py_{60}-Alm_{40} 100 K 293 K	Py_{20}-Alm_{80} 100 K 293 K	Almandine 100 K 293 K
			Tetrahedron		
4 × Si-O	100 K 1.6343(1)	1.636(1)	1.6373(8)	1.637(2)	1.6364(3)
	293 K 1.6342(3)	1.635(1)	1.6355(4)	1.634(2)	1.6352(4)
2 × (O1-O2)	100 K 2.4984(3)	2.501(1)	2.509(1)	2.509(3)	2.5134(4)
(shared edge)	293 K 2.4965(3)	2.500(2)	2.504(1)	2.507(3)	2.5090(6)
2 × O1-Si-O2	100 K 99.70(1)	99.68(5)	100.02(4)	100.02(8)	100.34(1)
	293 K 99.61(1)	99.73(6)	99.90(3)	100.15(8)	100.21(1)
4 × (O1-O3)	100 K 2.7499(3)	2.753(1)	2.752(1)	2.753(3)	2.7483(4)
(unshared edge)	293 K 2.7507(3)	2.751(2)	2.750(1)	2.747(3)	2.7472(6)
4 × O1-Si-O3	100 K 114.57(1)	114.58(5)	114.40(4)	114.39(8)	114.22(1)
	293 K 114.62(1)	114.55(6)	114.46(3)	114.32(8)	114.29(1)
Mean O-O	100 K 2.6661	2.6690	2.6710	2.6717	2.6700
	293 K 2.6660	2.6673	2.6680	2.6670	2.6678
ELD (%)*	100 K 4.19(1)	4.20(4)	4.04(4)	4.06(12)	3.91(2)
	293 K 4.24(1)	4.18(4)	4.10(4)	4.00(12)	3.97(3)
O-T-O	100 K 58.99	59.23	55.16	55.09	51.39
Angle variance**	293 K 60.11	58.59	56.55	53.56	52.88
α (rotation)†	100 K 27.66(1)	27.62(5)	27.34(4)	27.22(8)	26.93(1)
	293 K 27.50(1)	27.43(6)	27.22(3)	26.82(9)	26.75(1)
			Octahedron		
6 × Al-O	100 K 1.8853(1)	1.888(1)	1.8856(8)	1.891(2)	1.8882(3)
	293 K 1.8862(3)	1.889(1)	1.8881(4)	1.890(2)	1.8904(4)
6 × (O1-O4)	100 K 2.6136(3)	2.618(1)	2.620(1)	2.632(3)	2.6362(4)
(shared edge)	293 K 2.6165(3)	2.624(2)	2.627(1)	2.640(3)	2.6422(6)
6 × O1-Al-O4	100 K 87.76(1)	87.79(5)	88.02(4)	88.22(8)	88.54(1)
	293 K 87.86(1)	87.99(6)	88.18(3)	88.57(8)	88.67(1)
6 × (O4-O5)	100 K 2.7178(3)	2.721(1)	2.712(1)	2.715(3)	2.7042(4)
(unshared edge)	293 K 2.7161(3)	2.718(2)	2.712(1)	2.707(3)	2.7044(6)
6 × O4-Al-O5	100 K 92.24(1)	92.21(5)	91.98(4)	91.78(8)	91.46(1)
	293 K 92.14(1)	92.01(6)	91.82(3)	91.43(8)	91.33(1)
Mean O-O	100 K 2.6657	2.6695	2.6660	2.6735	2.6702
	293 K 2.6663	2.6710	2.6695	2.6710	2.6733
ELD (%)	100 K 1.95	1.92	1.91	1.55	1.28
	293 K 1.87	1.76	1.59	1.25	1.16
O-Al-O	100 K 5.47	5.33	4.28	3.46	2.33
Angle variance	293 K 5.00	4.41	3.61	2.23	1.93
			Cube dodecahdron		
4 × X-O2	100 K 2.1946(1)	2.199(1)	2.2067(8)	2.214(2)	2.2198(3)
	293 K 2.1974(3)	2.203(1)	2.2081(4)	2.218(2)	2.2208(4)
4 × X-O4	100 K 2.3336(1)	2.338(1)	2.3442(8)	2.356(2)	2.3634(3)
	293 K 2.3401(3)	2.346(1)	2.3525(4)	2.368(2)	2.3712(4)
Mean (X-O)	100 K 2.2641	2.2685	2.2755	2.2850	2.2916
	293 K 2.2688	2.2745	2.2803	2.2930	2.2960
2 × (O1-O2)	100 K 2.4984(3)	2.501(1)	2.509(1)	2.509(3)	2.5134(4)
	293 K 2.4965(3)	2.500(2)	2.504(1)	2.507(3)	2.5090(6)
2 × (O4-O7)	100 K 2.7691(3)	2.775(1)	2.775(1)	2.786(3)	2.7864(4)
	293 K 2.7781(3)	2.781(2)	2.784(1)	2.793(3)	2.7963(6)
4 × (O1-O4)	100 K 2.6136(3)	2.618(1)	2.620(1)	2.632(3)	2.6362(4)
	293 K 2.6165(3)	2.624(2)	2.627(1)	2.640(3)	2.6422(6)
4 × (O4-O6)	100 K 2.6995(3)	2.705(1)	2.752(1)	2.753(3)	2.7560(4)
	293 K 2.7079(3)	2.718(2)	2.750(1)	2.757(3)	2.7643(6)
Mean O-O	100 K 2.6490	2.6537	2.6713	2.6775	2.6807
	293 K 2.6539	2.6608	2.6737	2.6823	2.6864
σ^4	100 K 53.18	53.20	53.35	53.49	53.71
	293 K 53.23	53.32	53.46	53.75	53.80
ϕ^4	100 K 3.38	3.38	3.38	3.49	3.52
	293 K 3.50	3.51	3.54	3.68	3.67

* Defined by Renner and Lehmann (1986).
** Defined by Robinson et al. (1971).
† Defined by Born and Zemann (1964).
‡ Defined by Euler and Bruce (1965).

sitions is within 3σ of the refined coordinates. The largest differences between refined and predicted displacement parameters are observed for the U_{ij}'s of Py_{60}-Alm_{40} at *RT*, where a few of the refined displacement parameters are up to 5σ higher than the calculated values. Such differences are characteristic of data having a relatively low upper-θ limit (Armbruster et al., 1990), 40° in this case. All other displacement parameters are within 4σ of the model values. In summary, the agreement between model and measured displacement parameters is satisfactory. One small systematic deviation however is observed: at 100 and 293 K, refined U_{12}(Mg,Fe) displacement param-

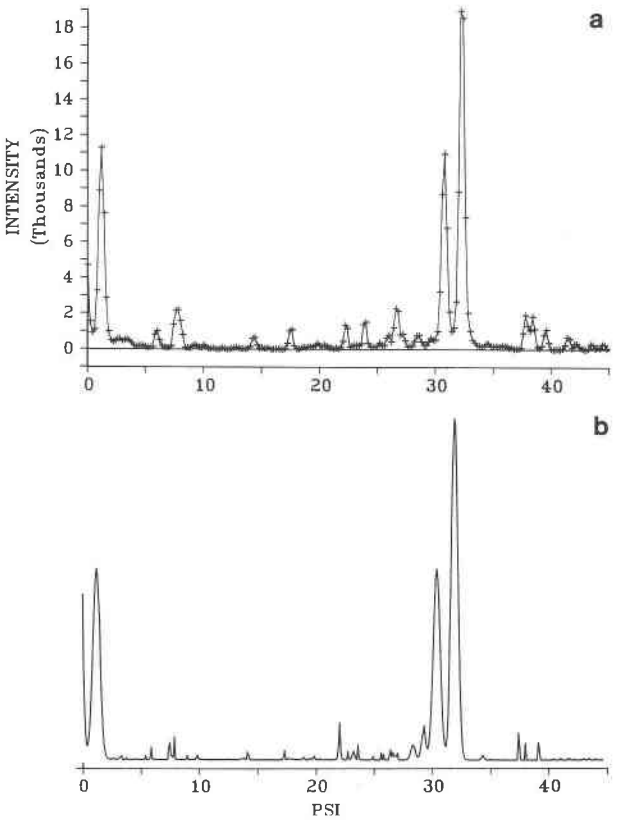

Fig. 1. Multiple reflection profile for the forbidden reflection 10,10,2 of pyrope at 293 K. Multiple reflection phenomena are characterized by a strong intensity variation with varying ψ angle: (**a**) measured intensity profile by stepwise variation of the ψ angle; (**b**) calculated ψ profile in space group $Ia\bar{3}d$ using the program PSIINT by Rossmanith et al. (1990).

eters are smaller than the interpolated values. In this respect, intermediate solid-solution garnet members behave more like almandine than like pyrope. This is likely an artifact for the intermediate pyrope-almandine solid solution compositions owing to the stronger scattering power of Fe compared with Mg.

Temperature dependence

The cell dimensions of pyrope and almandine increase 0.011 and 0.013 Å, respectively, between 100 and 293 K (Table 2). Solid-solution members do not show any significant deviation from this trend. The O y coordinate is temperature dependent, whereas no significant change between 100 and 293 K can be observed for the O x and z coordinates (Tables 4a, 4b). The change of y can be understood on the basis of the tetrahedral rotation, α, about the $\bar{4}$ axis (Figs. 2, 3), as first proposed by Born and Zemann (1964). When the Si cation is placed at the origin and x_O,y_O,z_O are the corresponding O coordinates (approximately at 0.091,−0.05,−0.097), the position of the tetrahedron can be described by the angle α, where $\tan \alpha = y_O/z_O$. Figure 3 shows the variation of the tetrahedral rotation angle as a function of chemical composition and temperature. It can be seen that α increases with increasing pyrope component and decreasing temperature. The rotation of the tetrahedron, about the $\bar{4}$ axis toward decreasing α values, has two important structural implications (Meagher, 1975): (1) the size of the dodecahedron (X site) increases, (2) X-O4 will increase more than X-O2 (positions O2 and O4 are shown in Fig. 2). In pyrope almandine garnets, the shorter (Mg,Fe^{2+})-O2 distance shows a slight increase (ca. 0.0025 Å) between 100 and 293 K. The longer (Mg,Fe^{2+})-O4 distance increases more, between 0.0078 and 0.0092 Å, from 100 to 293 K (Table 5). This effect becomes more pronounced toward the almandine end-member. The linear correlation between tetrahedral rotation and the longer X-O4 distance is shown in Figure 4. It is interesting to note that the correlation holds independent of whether the variation of α is caused by Mg → Fe^{2+} substitution or by a change of temperature. This effect has already been noted (Meagher, 1975) for the pyrope structure at elevated temperatures or with solid solution. This same relation holds also quantitatively for pyrope almandine garnets between 100 and 293 K.

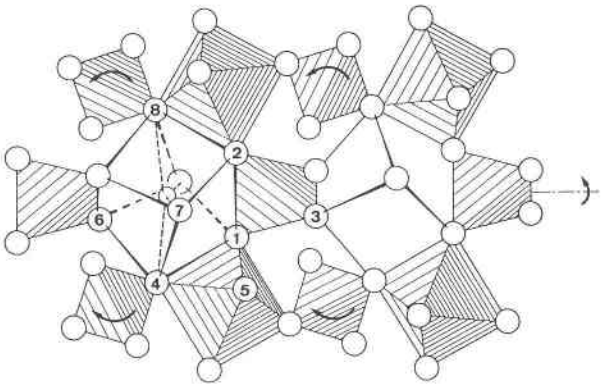

Fig. 2. Polyhedral model of the garnet structure projected down the c axis (modified after Gibbs and Smith, 1965). Numbers on O atoms refer to the X-O and O-O distances of Table 5. X-O4 and symmetry-equivalent bond distances are longer compared with X-O2. The arrows show the effect that tetrahedra rotation has on the relative length of AlO_6 and XO_8 polyhedral edges. The tetrahedra are shown rotating to smaller α values.

Novak and Gibbs (1971) showed through linear regression analysis that the angle ϕ, introduced by Euler and Bruce (1965), is a good measure of dodecahedral distortion. The value of ϕ increases generally with temperature and becomes greater toward almandine (Table 5). The Si-O tetrahedral bond distances do not change measurably with temperature (Table 5). The O1-Si-O2 angle (ca. 100°), between the O atoms related by the twofold axis (Table 5), can be calculated (Born and Zemann, 1964) as $\cos(\text{O1-Si-O2}/2) = a \cdot x_O/\text{d(Si-O)}$. Because x_O is temperature independent between 100 and 293 K, this angle decreases approximately 0.1° as a function of the unit-cell parameter change. Therefore, the angular distortion of the tetrahedron increases with temperature, whereas

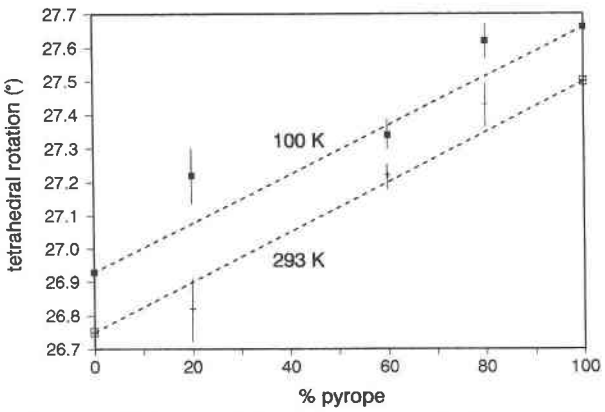

Fig. 3. Rigid tetrahedral rotation (Born and Zemann, 1964) as function of the pyrope component at 100 and 293 K for almandine-pyrope solid solutions. Dotted lines connect rotation angles for end-member almandine and pyrope. Standard deviations of the end-member pyrope and almandine coincide with the heights of the symbols.

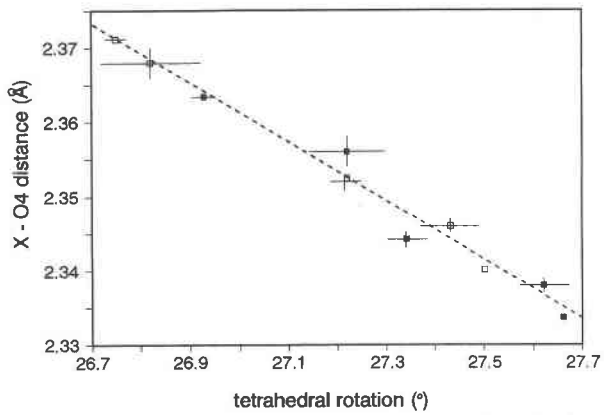

Fig. 4. The long X-O4 distance as function of the rigid tetrahedral rotation (α) about the fourfold axis. This inverse correlation exists for data at both 100 K (filled squares) and 293 K (open squares).

the angular distortion of the octahedron behaves in an opposite manner (Table 5). The edge-length distortion of the tetrahedron (ELD) increases slightly with increasing temperature but decreases for the octahedron. The same general trend is seen for the angular variances (Table 5) defined by Robinson et al. (1971), confirming the results of Meagher (1975) for pyrope. The angular distortion of the octahedron is smaller in almandine than in pyrope. The octahedron shows a positive expansion, with an Al-O distance increasing from 100 to 293 K. This effect is especially pronounced for almandine.

The ^{57}Fe Mössbauer hyperfine parameters of synthetic almandine pyrope garnets have been measured at 293 and 77 K (Geiger et al., 1990). This spectroscopic information, which is specific to the Fe dodecahedral site, can be compared with these X-ray diffraction data. A slight linear increase in the quadrupole splitting (QS) from 3.54(1) to 3.59(1) mm/s at 293 K was recorded progressing from end-member almandine to pyrope-rich ($Py_{90}Alm_{10}$) compositions. This trend is consistent with the greater average dodecahedral site distortion with increasing almandine component in the solid-solution compositions as determined by diffraction methods. Quadrupole splittings at 77 K are slightly greater than those measured at 293 K but are similar across the Alm-Py join [3.64(1) mm/s]. The temperature-dependent change in the QS is also consistent with the lower average dodecahedral site distortion measured here with decreasing temperature (Table 5). The constant values of the QS at 77 K are, however, partly inconsistent with the small changes in average site distortion measured at 100 K in the Alm-rich compositions. The isomer shifts recorded at 293 and 77 K are essentially constant for all compositions, indicating to a first degree that the bonding characteristics (e.g., ionic vs. covalent character) of Fe^{2+} in the eight-coordinated dodecahedral site do not change significantly as a function of bulk composition (Geiger et al., 1990).

An extremely useful and sensitive method for studying the temperature dependence of displacement parameters involves the evaluation of difference displacement amplitudes along the bonding vector (Bürgi, 1989). With increasing temperature a rigid coordination polyhedron exhibits increased displacement parameters of the central atom and the ligands; however, the averaged difference displacements (ΔU's) determined along the bonding vectors remain unchanged. Chandrasekhar and Bürgi (1984) and Kunz and Armbruster (1990) have demonstrated applications of this method and discussed the theoretical background. In the structures reported here the SiO_4 tetrahedra and AlO_6 octahedra behave as rigid polyhedra and show no temperature dependence for ΔU in all compositions. In contrast, the dodecahedral (X) site displays nonrigid behavior, with ΔU values along the longer X-O4 bond increasing with temperature (Fig. 5), whereas ΔU values along the shorter distance (X-O2) remain unchanged. This can be explained in terms of dynamic disorder of the X cation within the plane defined by the four O atoms with the long X-O4 bonds (Geiger et al., 1992). The amplitude of this motion is greater and more temperature dependent for pyrope than for almandine (Table 6) and may be related to the smaller atomic weight of Mg compared with Fe (Fig. 5).

Relationship to thermodynamic properties

A satisfactory standard activity-composition model addressing the enthalpies, entropies, and volumes of mixing for the aluminosilicate garnets does not exist, and there is disagreement regarding interpretations of the significance of the experimental data. These diffraction data allow inferences to be made concerning the energetics of almandine-pyrope solid solutions measured at 1033 K by solution calorimetry (Geiger et al., 1987). The atomic co-

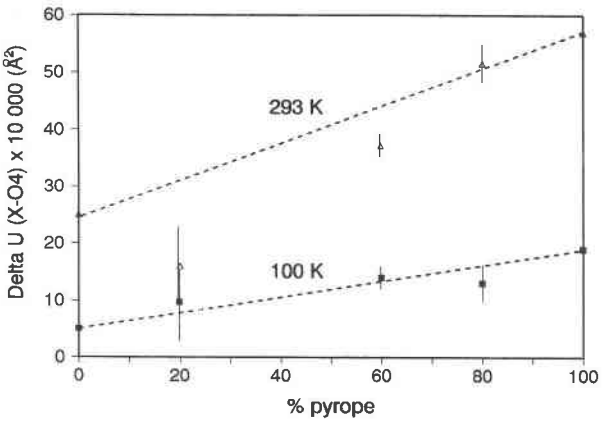

Fig. 5. The difference mean-square-displacement parameters [ΔU (Å^2)], evaluated at 100 and 293 K along the X-O4 distance, are plotted vs. the pyrope component. Dashed lines connect the end-members. Standard deviations for the end-member pyrope and almandine coincide with the heights of the symbols.

ordinates and atomic displacement parameters show no major discontinuities or breaks across the join, but instead they vary in a relatively linear fashion. Therefore, we find no apparent structural elastic strains that could account for any positive excess enthalpies of mixing for almandine pyrope garnets.

The vibrational behavior of the atoms in the garnet structure also allows one to consider the possible nature of the third-law entropies across the almandine-pyrope join and to determine whether any excess entropies of mixing are present in almandine pyrope garnets. The existing proposals for excess entropies (as determined from model-dependent calculations, phase equilibrium data, and calorimetry) are open to considerable discussion. Some thermodynamic models give asymmetric excess entropies of mixing (e.g., Bhattacharya et al., 1991) and are, in many cases, strongly dependent on the fitting model adopted for the heats of solution measured on almandine pyrope garnets (Geiger et al., 1987). Strictly from ionic size considerations, however, the exchange of Mg and Fe^{2+} cations in the dodecahedral site, and the resultant small change in the molar volumes of mixing along this binary join, should give rise to little excess entropy of mixing (Geiger, 1986).

The difference-displacement parameters determined for the solid-solution compositions from this diffraction study do not indicate any unusual or excessive vibrations that would affect heat capacities in an overt manner, at least to 100 K. The X-ray data support the conjecture that the vibrational entropies of mixing across the almandine-pyrope join should be nearly ideal or have minimal excess nonideality. It is clear however that strong anisotropic vibration of the small divalent cations in the dodecahedral site gives rise to the relatively large heat capacities and large third-law entropies observed for pyrope and almandine (Geiger et al., in preparation). There has been only a single low-temperature calorimetric heat-capacity

Table 6. Difference mean-square-displacement parameters [ΔU = U(MET) − U(O) (Å^2)] evaluated along interatomic vectors in almandine pyrope garnets

Composition	Temp. (K)	Si-O (Å^2)	Al-O (Å^2)	X-O2 (Å^2)	X-O4 (Å^2)
Pyrope	100	−0.0004(1)	−0.0004	−0.0005	0.0019
	293	−0.0003(1)	−0.0004	−0.0003	0.0057
Py_{80}-Alm_{20}	100	−0.0008(3)	−0.0008	−0.0010	0.0011
	293	−0.0004(3)	−0.0009	−0.0007	0.0052
Py_{60}-Alm_{40}	100	−0.0004(4)	−0.0002	−0.0011	0.0014
	293	−0.0005(4)	−0.0007	−0.0003	0.0037
Py_{20}-Alm_{80}	100	−0.0003(6)	npd	−0.0019	0.0010
	293	−0.0001(6)	−0.0011	−0.0014	0.0013
Almandine	100	−0.0005(1)	−0.0005	−0.0017	0.0005
	293	−0.0003(1)	−0.0003	−0.0018	0.0025

Note: Standard deviations cited in the first column refer to the whole line; npd = nonpositive definite; O2 and O4 are labeled in Figure 2.

study of synthetic aluminosilicate garnets. Haselton and Westrum (1980) measured the heat capacities of end-member pyrope and grossular and a solid solution composition of $Py_{60}Gr_{40}$ from 10 to 350 K. Their data indicate that the excess heat capacities for the solid solution come from the low-temperature region below 120 K and are possibly related to the increased Mg vibration amplitude caused by an expansion of the garnet structure through incorporation of the larger volume grossular component in solid solution. A similar situation is unlikely in almandine-pyrope solid solutions because of the more similar radii of Fe^{2+} and Mg^{2+}.

These diffraction data do not give an answer to whether short-range ordering may occur in the garnet structure. Space group $Ia\bar{3}d$ requires complete disorder of Mg^{2+} and Fe^{2+} on the dodecahedral site, but the occurrence of short-range ordering and its effect on the configurational entropies is an open question for the aluminosilicate garnets and has yet to be experimentally addressed. Moreover, additional effects such as crystal-field stabilization energies need to be quantified before the microscopic properties and their effect on the macroscopic properties are better understood.

References cited

Allen, F.M., and Buseck, P.R. (1988) XRD, FTIR, and TEM studies of optically anisotropic grossular garnets. American Mineralogist, 73, 568–584.

Armbruster, Th., Bürgi, H.B., Kunz, M., Gnos, E., Brönnimann, St., and Lienert, Ch. (1990) Variation of displacement parameters in structure refinements of low albite. American Mineralogist, 75, 135–140.

Berman, R.G. (1990) Mixing properties of Ca-Mg-Fe-Mn garnets. American Mineralogist, 75, 328–344.

Bhattacharya, A., Krishnakumar, K.R., Raith, M., and Sen, S.K. (1991) An improved set of a-X parameters for Fe-Mg-Ca garnets and refinements of the orthopyroxene-garnet thermometer and the orthopyroxene-garnet-plagioclase-quartz barometer. Journal of Petrology, 32, 629–665.

Born, L., and Zemann, J. (1964) Abstandsberechnungen und gitterenergetische Berechnungen an Granaten. Beiträge zur Mineralogie und Petrographie, 10, 2–23.

Bürgi, H.B. (1989) Interpretation of atomic displacement parameters: Intramolecular translational oscillation and rigid-body motion. Acta Crystallographica, B45, 383–390.

Chandrasekhar, K., and Bürgi, H.B. (1984) Dynamic processes in crystals

examined through difference vibrational parameters ΔU: The low-spin-high-spin transition in tris(dithiocarbamato)iron(III) complexes. Acta Crystallographica, B40, 387–397.

Cressey, C. (1981) Entropies and enthalpies of aluminosilicate garnets. Contributions to Mineralogy and Petrology, 76, 413–419.

Dempsey, M.J. (1980) Evidence for structural changes in garnet caused by calcium substitution. Contributions to Mineralogy and Petrology, 71, 281–282.

Dong, J., and Lu, K. (1991) Noncubic symmetry in garnet structures studied using extended X-ray-absorption fine-structure spectra. Physical Reviews B, 43, 8808–8821.

Enraf-Nonius (1983) Structure determination package (SDP). Enraf-Nonius, Delft, the Netherlands.

Euler, F., and Bruce, J.A. (1965) Oxygen coordinates of compounds with garnet structure. Acta Crystallographica, 19, 971–978.

Ganguly, J., and Saxena, S.K. (1984) Mixing properties of aluminosilicate garnets: Constraints from natural and experimental data, and applications to geothermobarometry. American Mineralogist, 69, 88–97.

Geiger, C.A. (1986) Thermodynamic mixing properties of almandine garnet solid solutions. Ph.D. thesis, University of Chicago, Chicago.

Geiger, C.A., Newton, R.C., and Kleppa, O.J. (1987) Enthalpy of mixing of synthetic almandine-grossular and almandine-pyrope garnets from high-temperature solution calorimetry. Geochimica et Cosmochimica Acta, 51, 1755–1763.

Geiger, C.A., Lottermoser, W., and Amthauer, G. (1990) A temperature dependent ^{57}Fe Mössbauer study of synthetic almandine-grossular and almandine-pyrope garnets: A comparison. Third International Symposium of Experimental Mineralogy, Petrology and Geochemistry, p. 11. Edinburgh, U.K.

Geiger, C.A., Rubie, D.C., Ross, C.R., II, and Seifert, F. (1991) A cation partitioning study of (Mg,Fe)SiO_3 garnet using ^{57}Fe Mössbauer spectroscopy. Eos, 72, 564–565.

Geiger, C.A., Armbruster, Th., Jiang, K., Lager, G.A., Lottermoser, W., and Amthauer, G. (1992) A combined temperature dependent ^{57}Fe Mössbauer and single crystal X-ray diffraction study of synthetic almandine: Evidence for the Goldanskii-Karyagin effect. Physics and Chemistry of Minerals, in press.

Geller, S. (1967) Crystal chemistry of the garnets. Zeitschrift für Kristallographie, 125, 1–47.

Gibbs, G.V., and Smith, J.V. (1965) Refinement of the crystal structure of synthetic pyrope. American Mineralogist, 50, 2023–2039.

Griffen, D.T., Hatch, D.M., and Phillips, W.R. (1990) Refinement of the structure of a natural tetragonal garnet. Geological Society of America Abstracts with Program, 22, A215.

Haselton, H.T., and Westrum, E.F., Jr. (1980) Low-temperature heat capacities of synthetic pyrope, grossular and $pyrope_{60}grossular_{40}$. Geochimica et Cosmochimica Acta, 44, 701–709.

Hirshfeld, F.L. (1976) Can X-ray data distinguish bonding effects from vibrational smearing? Acta Crystallographica, A32, 239–244.

Hofmeister, A.M., and Chopelas, A. (1991) Thermodynamic properties of pyrope and grossular from vibrational spectroscopy. American Mineralogist, 76, 880–891.

Ibers, J.A., and Hamilton, W.C., eds. (1974) International tables for X-ray crystallography, vol. 4, p. 99–101 and 149–150. Kynoch Press, Birmingham, England.

Kieffer, S.W. (1980) Thermodynamics and lattice vibrations of minerals: 4. Application to chain and sheet silicates and orthosilicates. Reviews of Geophysics and Space Physics, 18, 862–886.

Kingma, K.J., and Downs, J.W. (1989) Crystal-structure analysis of a birefringent andradite. American Mineralogist, 74, 1307–1316.

Kleber, W., Jost, K.H., and Ziemer, B. (1969) Zur Koordination des Magnesiums im Pyrop und Untersuchungen über dessen thermische Zersetzung. Kristall und Technik, 4, 423–429.

Kühberger, A., Fehr, T., Huckenholz, H.G., and Amthauer, G. (1989) Crystal chemistry of a natural schloromite and Ti-andradites synthesized at different oxygen fugacities. Physics and Chemistry of Minerals, 16, 734–740.

Kunz, M., and Armbruster, Th. (1990) Difference displacement parameters in alkali feldspars: Effects of (Si,Al) order-disorder. American Mineralogist, 75, 141–149.

Meagher, E.P. (1975) The crystal structures of pyrope and grossularite at elevated temperatures. American Mineralogist, 60, 218–228.

Megaw, H.D. (1968) A simple theory of the off-center displacement of cations in octahedral environments. Acta Crystallographica, B24, 149–153.

Menzer, G. (1928) Die Kristallstruktur der Granate. Zeitschrift für Kristallographie, 69, 300–396.

Novak, G.A., and Gibbs, G.V. (1971) The crystal chemistry of the silicate garnets. American Mineralogist, 56, 791–825.

Prandl, W. (1971) Die magnetische Struktur und die Atomparameter des Almandins $Al_2Fe_3(SiO_4)_3$. Zeitschrift für Kristallographie, 134, 333–343.

Renner, B., and Lehmann, G. (1986) Correlation of angular and bond length distortion in TO_4 units in crystals. Zeitschrift für Kristallographie, 175, 43–59.

Robinson, K., Gibbs, G.V., and Ribbe, P.H. (1972) Quadratic elongation: A quantitative measure of distortion in coordination polyhedra. Science, 172, 567–570.

Rossmanith, E., Klumpat, G., and Schulz, A. (1990) N-beam interactions examined with the help of the computer programs PSIINT and PSILAM. Journal of Applied Crystallography, 23, 99–104.

Takéuchi, Y., Haga, N., Umizu, S., and Sato, G. (1982) The derivative structure of silicate garnets in grandite. Zeitschrift für Kristallographie, 158, 53–99.

Winter, J.K., Ghose, S., and Okamura, F.P. (1977) A high temperature study of the thermal expansion and anisotropy of the sodium atom in low albite. American Mineralogist, 62, 921–931.

Yakel, H.L., and Fankuchen, I. (1962) Systematic multiple diffraction in equi-inclination Weissenberg geometry. Acta Crystallographica, 15, 1188.

Zemann, A., and Zemann, J. (1961) Verfeinerung der Kristallstruktur von synthetischem Pyrop, $Mg_3Al_2(SiO_4)_3$. Acta Crystallographica, 14, 835–837.

Zucker, U.H., Perenthaler, E., Kuhs, W.F., Bachmann, R., and Schulz, H. (1983) PROMETHEUS: A program system for investigation of anharmonic thermal vibrations in crystals. Journal of Applied Crystallography, 16, 358.

Manuscript received July 31, 1991
Manuscript accepted December 7, 1991